Wave Optic Analysis of Fizeau Fringes with Plate Defects.

J.M.Vaughan & K.D.Ridley

Optical & Lidar Associates, Pound Farm,
Cadmore End, Bucks HP14 3PF.

Abstract: In certain circumstances rigorous wave optic analysis of Fizeau fringe formation becomes essential. Results of such analysis are discussed together with the impact on spectroscopic measurements of frequency shift and width. Comparison is made with Fabry Perot performance.

1. Introduction.

In the Fizeau Interferometer light is successively reflected between the surface coatings of the two plates set at the required wedge angle. Multiple interference takes place leading ideally to straight line fringes parallel to the wedge vertex. Unlike the Fabry Perot Interferometer these fringes are localised close to the plate surfaces and are often described as 'fringes of equal thickness'. In the ray optic approximation the fringes may be considered to trace out the loci of constant path separation between the plates – thus giving straight line fringes for ideally flat plates. In practice of course plates are not absolutely flat, however minor defects of order λ/100 across the plates are usually considered as adding to the fringe width in a relatively minor and acceptable degree. Detailed analysis of Fizeau fringes has long been carried out by techniques of ray optics as given for example in the classical text of Born and Wolf[1] drawing on the analysis of Brossel[2] and developed by many subsequent authors[3,4,5,] In the basic ray optic approximation a simple geometric calculation is made for the paths of the successively reflected optical beams. From this the phase difference between the p^{th} ray and the directly transmitted ray is calculated and the successive amplitude/phase terms derived. The fringe intensity is then found by vector summation of these terms and squaring the resultant. It should be noted that in the simple ray optic approximation no allowance is made for local slope and no account is taken of diffraction effects.

The present subject of investigation is the Fizeau spectrometer of the ALADIN Dopplar wind lidar instrument[6] on board the ESA ADM/AEOLUS Mission. The plates selected for the spectrometer were polished by the relatively new technique of Magneto – Rheological Finishing (MRF)[7,8] In this technique the surface is polished by tracing over the optical element with a comparatively small region of magnetically stiffened cutting medium. For circular Fizeau plates the cutting medium was traced in a spiral pattern across the surface; with the MRF technique a surface finish/roughness of less than 1nm is expected. Optical examination and tests show that the overall flatness and smoothness of the plates fell within the specification of better than λ/100, equivalent to~ 4nm. However detailed interferometric examination showed clear evidence of a regular character to the defects with a circular, ring-like structure. These successive rings/spirals appear to be centred approximately at the centre of the plates; initial estimates (later revised) suggested that the pitch (ie the radial distance between the rings) was about 1mm with a depth of about +- 4nm. This 1mm pitch is in fact consistent with the cutting interval of the MRF polishing technique as it spirals over the plate. Classical techniques of polishing are very different; defects of λ/100 might be expected, but spread in a single cycle across the full area of the plates to give a weak departure from flatness – often described as 'dishing' or 'bowing'. In the MRF technique, however, it seems that the plate surface is much more rapidly corrugated with a peak to valley distance for the defects of order 0.5mm.

Examination of the Fizeau fringes formed between the plates revealed two rather unusual findings;

1.1 Firstly the fringes, rather than being generally uniform and approximately straight lines, were in fact strongly modulated and appeared to be broken up along their length into regions of high and low intensity.

1.2 Secondly as the input frequency was varied so that the fringe moved laterally across the plates, these regions of high and low intensity traced out what appeared to be equi-spaced circular rings with centre close to the centre of the plates.

Against this background it became imperative to examine the spectroscopic performance of the Fizeau instrument and the potential impact of the plate defects. This was carried out initially by ray optic analysis and then by a full rigorous wave optic treatment.

2. Ray Optic Analysis

As a first step loci of equal path separation were evaluated for several model plate surfaces. Figure 1 shows a more extreme example with circular defects supposed as ± 4nm (PtV) circular defects on both plates. The plate size is 36mm diameter and the wedge angle is 4.8μm.

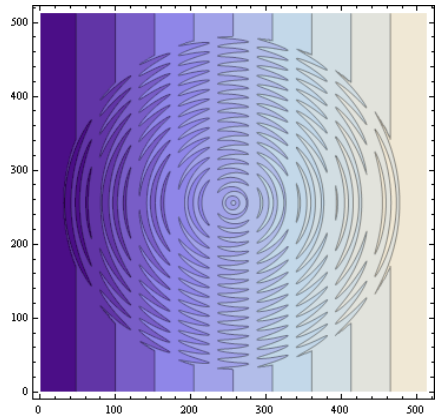

Figure 1: loci of equal path separation for plates with circular defects. The axes are in pixels of size 80μm to give the following physical parameters:

Plate size: (482-30)×0.08mm=36.1mm

Width of central equi-spaced contour;
Δx≈ (278-236)×0.08mm=3.36mm

Width x wedge angle;
3.36mm×4.8μrad=16.1nm≈4×4nm

As clear from the figure, the loci of equal path separation have a lateral (i.e., sideways to the vertical axis) spread of 3.36mm as the slope of the wedge compensates for the PtV groove defects on the plates.

Following this, calculations of the expected fringes with the ray optic approximation were made for a wide variety of modelled defects. Figure 2 shows an example, comparable to Figure 1. For this calculation the pixel spacing has been reduced to 50μm for 512 x 512 sampling so that an effective area on the plate of 25.6mm is sampled. The figure on the left hand side is with the full Born and Wolf[1] expression for the phase delay given by

$$\delta_p = \frac{4\pi}{\lambda} h\cos(\theta)\frac{\sin[(p-1)\alpha]}{\tan(\alpha)}\{\cos[(p-1)\alpha] - \tan(\theta)\sin[(p-1)\alpha]\} \quad \text{.....1}$$

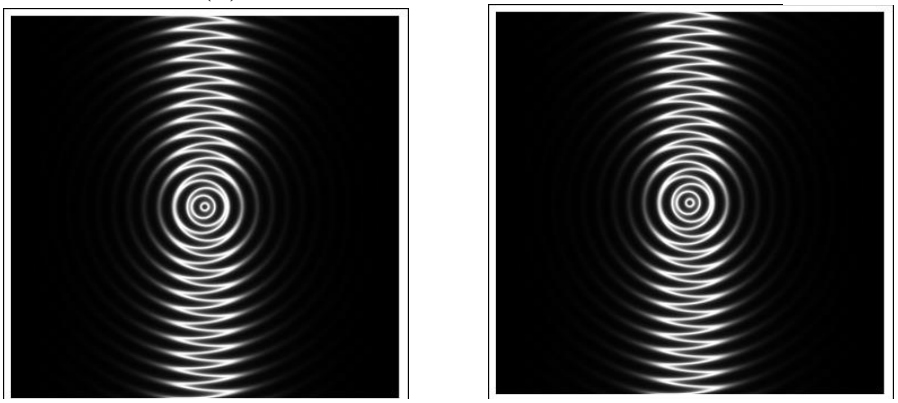

Figure 2: Fizeau fringes calculated for normal incidence, plate reflectivities 86%, plate separation 68.4mm and with incident frequency at the centre of the plate (nominal 0 MHz).

On the right hand side the small wedge approximation given by $\delta_p = \frac{4\pi}{\lambda} h(p-1)\cos(\theta)$ .....2 has been used. It is immediately apparent that the full Born and Wolf formula and the small wedge approximation give essentially the same result and are very similar to the loci of Figure 1 above. Most importantly, however, the fringes are continuous, not broken up, and their appearance is quite unlike those found experimentally as noted in 1.1 above.

3. Wave Optic Analysis

In the wave optic analysis the propagation of light between the reflective plates Z_0 and Z_1 is simulated by solving the paraxial wave equation for monochromatic radiation:

$$\frac{\partial^2 E}{\partial x^2} + \frac{\partial^2 E}{\partial y^2} - 2ik\frac{\partial E}{\partial z} = 0 \quad \text{.....3}$$

where $k = 2\pi/\lambda$. The wave equation can be solved by taking the spatial Fourier transform of E. In the Fourier domain, the solution is

$$e(\mathbf{\Omega}, z_1) = e(\mathbf{\Omega}, z_0)\exp\left[\frac{i|\mathbf{\Omega}|^2(z_1 - z_0)}{2k}\right] \qquad \text{.....4}$$

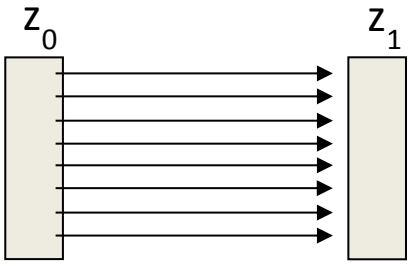

Figure 3: Propagation between plates

where e is the 2D Fourier transform of E, and $\mathbf{\Omega}$ is the spatial frequency vector. The solution in the spatial domain is found by inverse Fourier Transform. The algorithm is implemented by efficient Fast Fourier Transforms – see for example, Jakeman and Ridley[9]. Wave optic simulation with the same parameters as for Figure 2 are shown in Figure 4 below. The differences are immediately obvious: the fringes are now distinctly broken up and show a brighter region on the left hand side with a diffuse weaker system on the right hand side.

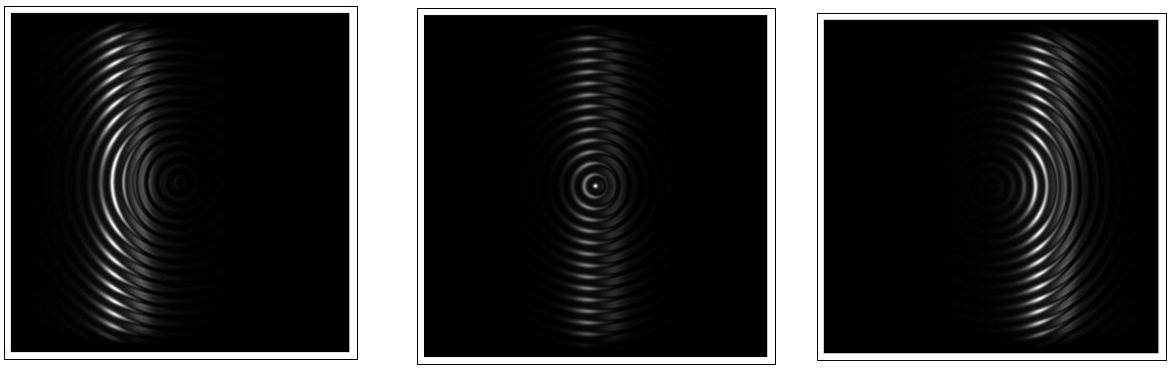

Figure 4: Wave optic simulation with relative input frequencies ± 300MHz, 0MHz (at the centre) and -300MHz

4. Calculation of Fringe Profiles and Line Shift

The fringe profiles were obtained by summation of the intensities in each pixel column. For the larger defects as in Figure 4, the resultant profiles were very asymmetric. As shown in Figure 5, fringe shifts and widths were

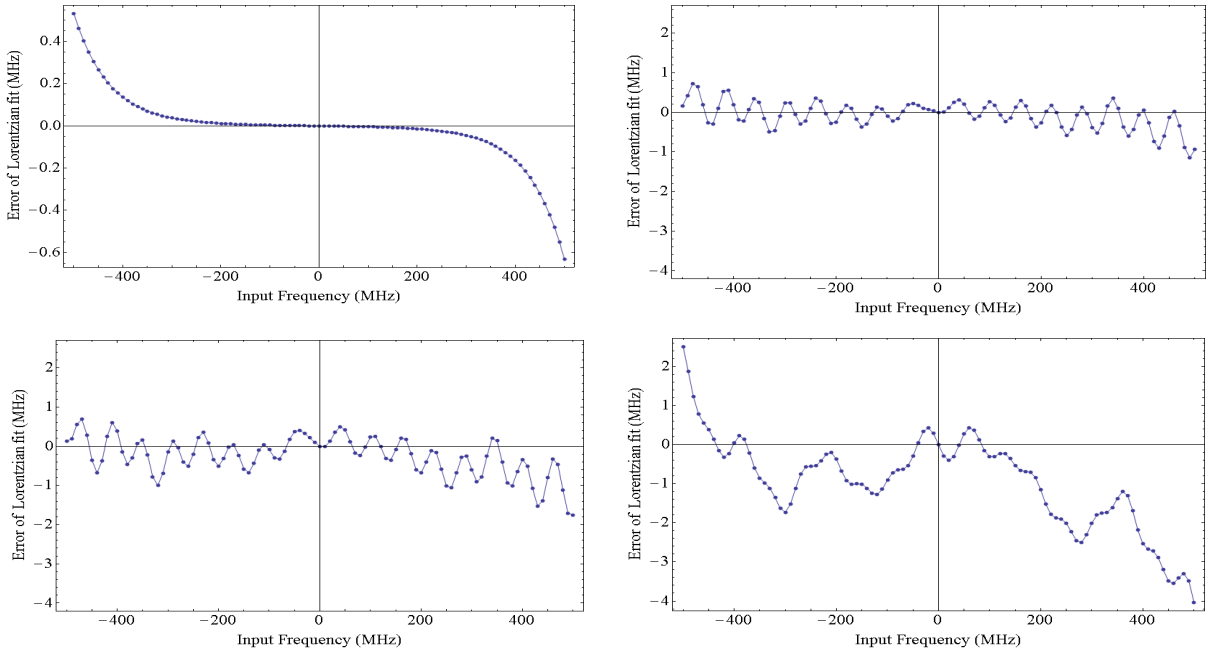

Figure 5: Lorentzian fit to the simulated fringes for a range of defects: top left perfect plates; top right ± 1nm defect; lower left ± 2nm defect; lower right ± 4nm defect. For perfect plates the frequency error is less than 0.1 MHz over the frequency range ± 400 MHz: the roll-off on either side (top left figure) is due to edge effects.

obtained with a best Lorentzian fit. The set of results shown in Figure 5 give the differences between the calculated position of the simulated fringe and the known input frequency, and also gave rapid changes of line width. Modulation due to the circular/spiral plate defects is immediately obvious.
Following this, a wave optic simulation was made using the best available data for the measured topography of the Fizeau plates. The resultant fringes appeared very similar to those found experimentally. The results for line shift and width with a Lorenzian fit are given in Figure 6 and show the impact due to the groove defects and larger scale aberrations. In actual experimental use, the integration of the spectra by detection into discrete frequency channels is required. This introduces a further complexity due to the width of these channels and this too has been investigated. In particular it requires careful evaluation of the analytic algorithm and the impact of defect-induced asymmetry of the fringe profile.

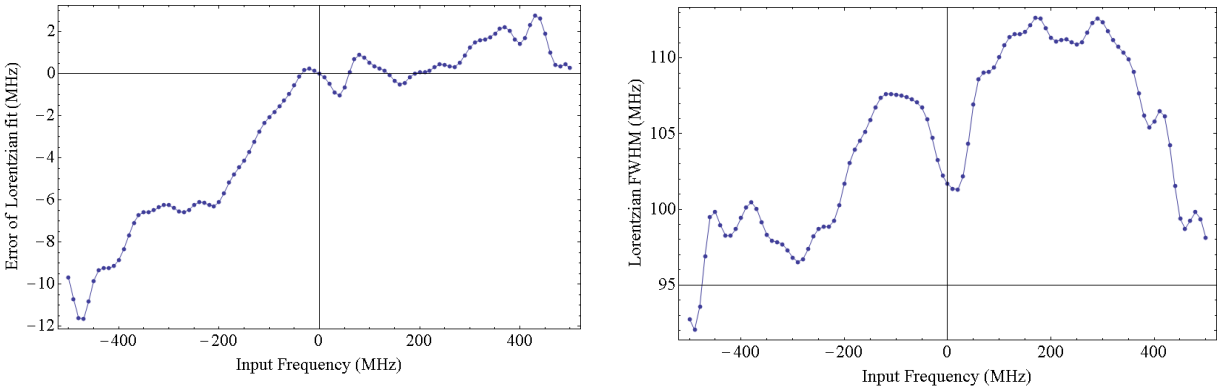

Figure 6: Frequency error and line width simulated for the actual Fizeau plates, plate reflectivity set at 88% and frequency scan at 10 MHz steps.

5. Conclusions and Comparison with the Fabry Perot Interferometer.

It is clear that surface defects in the Fizeau wedge interferometer can induce potentially significant errors in frequency and line width measurements which require to be evaluated by analysis and calibration.
In the Fabry Perot interferometer the fringes are localised in the focal plane of the fringe forming lens. This collects light across the whole plate aperture and the surface defects are thus effectively integrated across the full surface – see, e.g. section 3.6, Vaughan[10]. For the present plates with a reflectivity finesse of ~ 20 the effective defect finesse might be estimated at 40 or larger. This could lead to a uniform fringe broadening of 20 to 30%, but otherwise would have little impact on the spectroscopic performance.

6. Acknowledgments.

This work was funded by the European Space Agency under contract P.O. 5401001330. We are grateful to Alain Culoma of ESTEC and Eric Jakeman of Nottingham University for valuable discussion and comments on this investigation.

7. References

1. M. Born and E. Wolf, Principles of Optics (1959) (p. 351, 5th edition 1975, Pergamon Press)
2. J. Brossel, 'Multiple Beam Localised Fringes: 1 – Intensity Distribution and Localisation. 2 – Conditions of Observation and Formation of Ghosts'. Proc. Phys. Soc**., 59** 224, 234 (1947)
3. Y.H. Meyer, 'Fringe shape with an interferential wedge', J. Opt. Soc. Am., **71**, 1255 (1981)
4. T.T. Kajava, H.M. Lauranto and R.R.E Salomaa, 'Fizeau interferometer in spectral measurements', J. Opt. Soc. Am., **B10**, 1980 (1993)
5. J. McKay, 'Assessment of a multibeam Fizeau wedge interferometer for Doppler wind lidar', Applied Optics, **41**, 1760 (2002)
6. L. Francou et al, 'Optical analysis and performance verification on ALADIN spectrometers', Proc 7th ICSO (International Conference on Space Optics), Toulouse, France 2008.
7. S.D. Jacobs et al, Magnetorheological Finishing a Deterministic Process for Optics Manufacturing, LLE Review, **63**, 135 (1995)
8. D.C. Harris, 'History of Magnetorheological Finishing', Proc. SPIE WDTMXII, 8016, (2011)
9. E. Jakeman and K. Ridley, 'Modelling Fluctuations in Scattered Waves', Taylor and Francis (2006)
10. J.M. Vaughan, 'The Fabry Perot Interferometer', Adam Hilger, Taylor and Francis (1989)